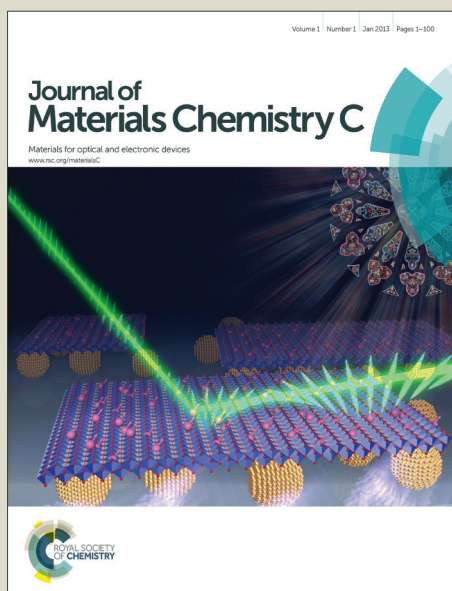


Journal of Materials Chemistry C

Accepted Manuscript



This is an *Accepted Manuscript*, which has been through the Royal Society of Chemistry peer review process and has been accepted for publication.

Accepted Manuscripts are published online shortly after acceptance, before technical editing, formatting and proof reading. Using this free service, authors can make their results available to the community, in citable form, before we publish the edited article. We will replace this *Accepted Manuscript* with the edited and formatted *Advance Article* as soon as it is available.

You can find more information about *Accepted Manuscripts* in the [Information for Authors](#).

Please note that technical editing may introduce minor changes to the text and/or graphics, which may alter content. The journal's standard [Terms & Conditions](#) and the [Ethical guidelines](#) still apply. In no event shall the Royal Society of Chemistry be held responsible for any errors or omissions in this *Accepted Manuscript* or any consequences arising from the use of any information it contains.

Fabrication of flexible polymer-GaN core-shell nanofibers by the combination of electrospinning and hollow cathode plasma-assisted atomic layer deposition

Cite this: DOI: 10.1039/x0xx00000x

Received 00th January 2012,
Accepted 00th January 2012

DOI: 10.1039/x0xx00000x

www.rsc.org/

Cagla Ozgit-Akgun,^{*ab} Fatma Kayaci,^{ab} Sessa Vempati,^a Ali Haider,^{ab} Asli Celebioglu,^{ab} Eda Goldenberg,^a Seda Kizir,^{ab} Tamer Uyar^{ab} and Necmi Biyikli^{*ab}

Here we demonstrate the combination of electrospinning and hollow cathode plasma-assisted atomic layer deposition (HCPA-ALD) processes by fabricating flexible polymer-GaN organic-inorganic core-shell nanofibers at a processing temperature much lower than those needed for the preparation of conventional GaN ceramic nanofibers. Polymer-GaN organic-inorganic core-shell nanofibers fabricated by the HCPA-ALD of GaN on electrospun polymeric (nylon 6,6) nanofibers at 200 °C were characterized in detail using electron microscopy, energy dispersive X-ray analysis, selected area electron diffraction, X-ray diffraction, X-ray photoelectron spectroscopy, photoluminescence measurements, and dynamic mechanical analysis. Although transmission electron microscopy studies indicated that the process parameters should be further optimized for obtaining ultimate uniformity and conformality on these high surface area 3D substrates, HCPA-ALD process resulted with a ~28 nm thick polycrystalline wurtzite GaN layer on polymeric nanofibers of an average fiber diameter of ~70 nm. Having flexible polymeric core and low processing temperature, these core-shell semiconducting nanofibers might potentially substitute brittle ceramic GaN nanofibers, which have already shown to be high performance materials for various electronic and optoelectronic applications.

Introduction

During the last few decades, gallium nitride (GaN), which is probably the most important semiconductor other than silicon, has been frequently used in optoelectronic devices operating in the blue region of the spectrum. GaN has a direct and relatively large band gap of 3.4 eV, high bond strength, good thermal conductivity, and high breakdown field. Therefore it is suitable for high power devices, as well as other devices operating at high temperatures and/or hostile environments.¹ Besides their thin film counterparts, also one-dimensional (1D) semiconducting GaN nanostructures have recently attracted much attention due to their potential applications in various device structures.² Single crystal or polycrystalline GaN nanostructures such as nanobelts, nanowires, or nanotubes with high aspect ratios were synthesized using different strategies including vapor-liquid-solid crystal growth,^{3,4,5,6,7,8} laser-assisted catalytic growth,^{9,10} template synthesis,^{11,12} and etching.^{13,14} Synthesis of randomly oriented or aligned continuous polymorphic GaN nanofibers having wurtzite structure was also demonstrated

by few research groups. These reports are electrospinning-based processes, where the electrospun composite nanofibers containing polymer and Ga precursor were subjected to calcination for the removal of organic components and subsequent high temperature (≥ 850 °C) nitridation in ammonia atmosphere.^{15,16,17,18,19,20,21} These GaN nanofibers (crystallite sizes < 20 nm) exhibited cathodoluminescence¹⁹ and photoconductivity,²⁰ and were successfully applied in UV detection²⁰ and ethanol sensing.²¹

Several research groups combined electrospinning and atomic layer deposition (ALD) to synthesize hollow inorganic nanofibers (or nanotubes) of Al₂O₃,²² AlN,²³ AlN/BN,²⁴ HfO₂,²⁵ SnO₂,^{26,27} TiO₂,^{28,29} TiO₂/ZnO,³⁰ and ZnO.^{31,32,33,34} Core-shell CuO-ZnO,³⁵ NiFe₂O₄-TiO₂,³⁶ polyacrylonitrile-ZnO,³⁷ SnO₂-ZnO,³⁸ TiO₂-ZnO,^{39,40} WO₃-TiO₂,⁴¹ and ZnO-TiO₂⁴⁰ nanofibers, Nb-doped TiO₂-supported Pt nanoparticle catalysts,⁴² and microtube-in-microtube ZnAl₂O₄ assemblies⁴³ were also fabricated successfully using this process combination. Recently our group synthesized photocatalytic polymer-ZnO core-shell nanofibers by the same approach.^{44,45,46,47} Besides showing

high photocatalytic activity the fabricated mats also easily handled and folded as a freestanding material due to the flexible polymeric core. Until recently, the fabrication of such flexible nanofibers with GaN shell has been limited by the absence of a low-temperature self-limiting ALD process for GaN. The temperatures required for the thermal ALD using metalorganic or halogenated Ga precursors were quite high to be compatible with polymeric substrates.^{48,49,50,51} In order to lower the reaction temperatures, NH₃ was activated via plasma during the trimethylgallium (GaMe₃)-NH₃ ALD process, however the resulting films were contaminated with ~20 at.% oxygen due to sputtering of the inductively coupled quartz plasma source.^{52,53} Recently, we deposited wurtzite GaN thin films with low impurity concentrations (O, C <1 at.%) in a self-limiting fashion at 200 °C using an ALD system coupled with hollow cathode plasma source.⁵⁴ (Opto)electronic properties of the GaN thin films were studied via fabricating transistors⁵⁵ and UV photodetectors.⁵⁶

Here we performed the fabrication of flexible polymer-GaN organic-inorganic core-shell nanofibers by the combination of electrospinning and hollow cathode plasma-assisted ALD (HCPA-ALD) processes. Following the fabrication of pristine polymeric (nylon 6,6) nanofibers with an average fiber diameter of ~70 nm by electrospinning, 1000 cycles of GaN were deposited on these nanofibers at 200 °C via HCPA-ALD using GaMe₃ and N₂/H₂ plasma as the Ga and N sources, respectively. Pristine nylon 6,6 and/or nylon-GaN core-shell nanofibers were characterized in detail using electron microscopy, energy dispersive X-ray analysis (EDX), selected area electron diffraction (SAED), X-ray diffraction (XRD), X-ray photoelectron spectroscopy (XPS), photoluminescence (PL) measurements and dynamic mechanical analysis (DMA).

Experimental

Fabrication of Polymer-GaN Core-Shell Nanofibers

Materials: Nylon 6,6 (relative viscosity 230,000–280,000) pellets and formic acid (98-100%) were purchased from Sigma-Aldrich. For the HCPA-ALD process, GaMe₃ purchased from Sigma-Aldrich, 5N-grade N₂ and H₂ gases, and Ar gas purchased from Linde were used as the Ga precursor, N-containing plasma gas, and carrier gas, respectively. N₂, H₂ and Ar gases were further purified using MicroTorr gas purifiers, while the other materials were used without any purification.

Electrospinning of Nylon 6,6 Nanofibers: 8 wt.% nylon 6,6 pellets were dissolved in formic acid for 3 h to yield a homogeneous clear solution. This solution was then loaded in a 3 ml syringe fitted with a metallic needle with ~0.8 mm inner diameter. Syringe was fixed horizontally on the syringe pump (KD Scientific, KDS 101) and polymer solution was pumped with a feed rate of 1 ml/h. Electrospinning of the solution was performed by applying a voltage of ~15 kV to the metal needle tip by a high voltage power supply (Matsusada Precision, AU Series). Tip-to-collector distance

was set to ~10 cm. The collector was wrapped with clean Al foil and grounded. As the solvent evaporates solidified nylon 6,6 nanofibers were deposited on the collector. The electrospinning setup was enclosed in a Plexiglas box which allowed electrospinning process to be carried out at 24 °C and 30% relative humidity.

Hollow cathode plasma-assisted ALD of GaN: HCPA-ALD of GaN was carried out at 200 °C in a Fiji F200-LL ALD reactor (Ultratech/Cambridge NanoTech Inc.) equipped with a remote stainless steel hollow cathode plasma source (Meaglow Ltd.). Prior to depositions, GaMe₃ cylinder was cooled to ~6 °C and stabilized at this temperature using a home-made Peltier system. Nylon 6,6 nanofibers collected on an Al foil (having a circular area of ~80 cm²) was fixed at the center of the substrate holder. The sample is loaded into the reactor via load-lock and maintained at the deposition temperature for at least 20 min before the process was initiated. GaMe₃ pulses and plasma gases were carried through separate lines at 30 and 100 sccm of Ar, respectively. The base pressure (with Ar carrier flows) was ~150 mTorr. 1000 cycles GaN was deposited, where one HCPA-ALD cycle consists of 0.015 s GaMe₃/10 s Ar purge/40 s 50/50 sccm N₂/H₂ plasma (300 W)/10 s Ar purge.

Characterization

Scanning electron microscopy (SEM) imaging of pristine nylon 6,6 and nylon-GaN core-shell nanofibers was performed using a FEI Quanta 200 FEG SEM. Prior to the imaging, ~5 nm Au/Pd alloy was sputter-deposited on SEM samples in a Precision Etching Coating System (PECS, Gatan, Model 682). Transmission electron microscopy (TEM), SAED, and EDX were carried out using FEI Tecnai G2 F30 TEM (operating at 300 kV). For these analyses, the sample was peeled off from its support (i.e., Al foil), dispersed in ethanol and drop-casted onto a Cu TEM grid. XRD patterns of the freestanding samples, which were placed carefully on a zero-background sample holder, were recorded in the range of 2Theta = 15–75° using PANalytical X'Pert Pro Multi Purpose X-ray diffractometer with Cu K α radiation (λ = 1.5418 Å). The step size and counting time were ~0.05° and 300 s (or 2000 s), respectively. Chemical composition and bonding states of the pristine nylon 6,6 and nylon-GaN core-shell nanofibers were investigated by XPS (Thermo Fisher Scientific) with a monochromatic Al K α radiation. The pass energy, step size, and spot size were 30 eV, 0.1 eV, and 400 mm, respectively. All spectra were corrected for charging by shifting peaks with respect to the adventitious C peak located at ~284.8 eV. Peak deconvolution was performed using the Avantage Software without applying any restrictions to spectral location and full width at half maximum values. PL measurements were carried out using a time-resolved fluorescence spectrophotometer (Jobin Yvon, model FL-1057 TCSPC) within the wavelength range of 300–500 nm. The excitation wavelength was ~270 nm. The dynamic mechanical analyzer (DMA, Q800 TA Instruments) was used to determine the mechanical performances of

pristine nylon 6,6 and nylon-GaN core-shell nanofibers. Measured samples were rectangular in shape, having an approximate size of ~ 10 mm (gap) \times ~ 2.5 mm (width) \times ~ 0.14 mm (thickness). The stress-strain curve of the nanofibrous web was obtained at a constant rate of 0.5 N/min and the average values were calculated by performing three measurements at room temperature. The storage modulus of the composite nanofibers was recorded in the range of 75–200 °C at a heating rate of 3 °C/min by applying an amplitude of 15 μ m.

Results and discussion

Representative SEM images of pristine nylon 6,6 nanofibers are given in Figures 1a and b. From these images, it is seen that the electrospinning process described in previous section resulted in bead-free polymeric nanofibers with a smooth morphology and uniform fiber diameter. Average fiber diameter for these pristine nylon 6,6 nanofibers was calculated by taking ~ 100 measurements from high magnification SEM images. The average value is 68 ± 12 nm, which is in good agreement with the values reported previously by us for the very same process.^{23,44} Figures 1c and d are the representative SEM images of nylon-GaN core-shell nanofibers at different magnifications. The images show that GaN layer was deposited in a very uniform and conformal fashion on the individual nylon 6,6 nanofibers without destroying the overall morphology. Average fiber diameter of nylon-GaN core-shell nanofibers was also calculated by averaging ~ 100 measurements from high magnification SEM images and found to be 123 ± 24 nm. Using this data the average film thickness for the deposited GaN was found to be ~ 27.5 nm which corresponds to a growth per cycle (GPC) value of ~ 0.28 Å. Previously, the growth of GaN on Si substrates (for a GaMe₃ pulse length of

0.03 s) was shown to be substrate-enhanced with a GPC of 0.47 Å for 75 cycles decreasing gradually to ~ 0.22 Å for 900 cycles.⁵⁴ Here, it should also be noted that the 0.015 s and 0.03 s of GaMe₃ pulse lengths both resulted in a similar GPC and thickness uniformity over 4 in. Si substrate (0.23 Å and $\pm 1.31\%$ vs. 0.22 Å and $\pm 0.77\%$).⁵⁴ Therefore, in this study GaMe₃ pulse length of 0.015 s was used in the first step of the HCPA-ALD cycle.

Representative TEM images of the nylon-GaN core-shell nanofiber(s) are shown in Figures 2a and b. From Figure 2a it is seen that a conformal GaN layer was formed on individual nanofibers with very uniform wall thicknesses along the fiber axis. In addition, the pristine nylon 6,6 nanofibers seem to be not affected neither by the process temperature nor the highly reactive precursors and plasma gases. Glass-transition (T_g) and melting (T_m) temperatures of electrospun nylon 6,6 nanofibers are reported to be 85 °C and 260 °C, respectively.⁵⁷ Moreover, thermal degradation of the nylon 6,6 nanofibers was not observed until 400 °C.⁴⁴ Although the process temperature (i.e., 200 °C) is above T_g , it is lower than both T_m and thermal decomposition temperature, which is shown to be low enough for the treatment of nanofibers without damaging their morphology. TEM investigation performed at higher magnifications revealed a relatively sharp nylon-GaN interface and did not show any contrast difference at subsurface region of the polymeric nanofiber indicating that GaMe₃ does not diffuse into the nylon 6,6 nanofibers during the process. Despite we acknowledge that further supporting data such TEM and EDX analysis of fiber cross-section are needed to verify this claim. Thickness of the GaN layer was precisely measured from the TEM image given in Figure 2b, and seen to vary between 23.3 nm and 26.8 nm along the fiber axis. Besides this $\pm 14\%$ variation in GaN wall thickness, TEM investigations also evidenced GaN layers that are thinner than expected on the nylon nanofibers (not shown here). A similar result is observed by us earlier in which AlN hollow nanofibers were fabricated by the deposition of an AlN layer on electrospun nylon 6,6 nanofibers via plasma-assisted ALD and subsequent calcination.²³ With its inherent self-limiting growth mechanism ALD is a very unique technique that results in the non-line-of-site deposition of highly uniform and conformal thin films even on 3D complex nanostructures such as electrospun nanofiber mats with sub-Å thickness control. However, as in every process, the parameters must be carefully optimized to achieve the best results. Uniformity and conformality of the deposited layer can be maximized by considering the requirements of gas-solid ALD reactions occurring at the substrate surface, and accordingly adjusting precursor doses, exposure time and purging time at a given reaction temperature. A right amount of precursor must be pulsed into the reactor; for insufficient amounts the conformality would be limited by the insufficient number of reactant molecules that results with unreacted surface sites, and for excess amounts the purging time may become

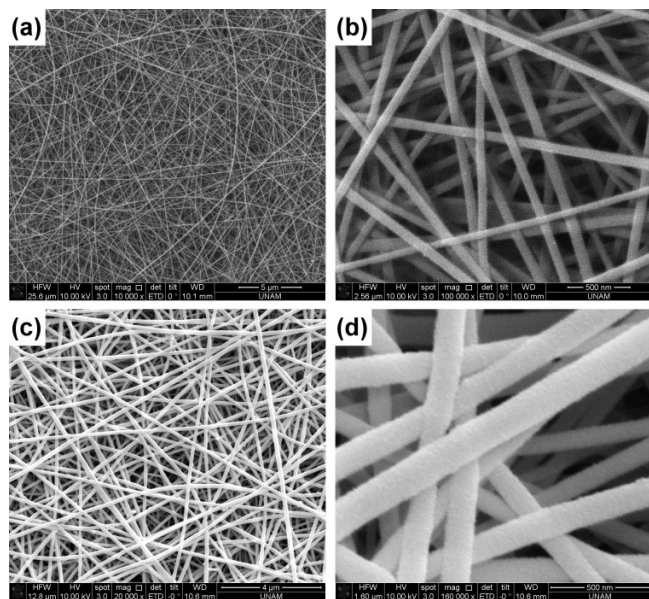


Figure 1. Representative SEM images of (a, b) pristine nylon 6,6, and (c, d) nylon-GaN core-shell nanofibers at different magnifications.

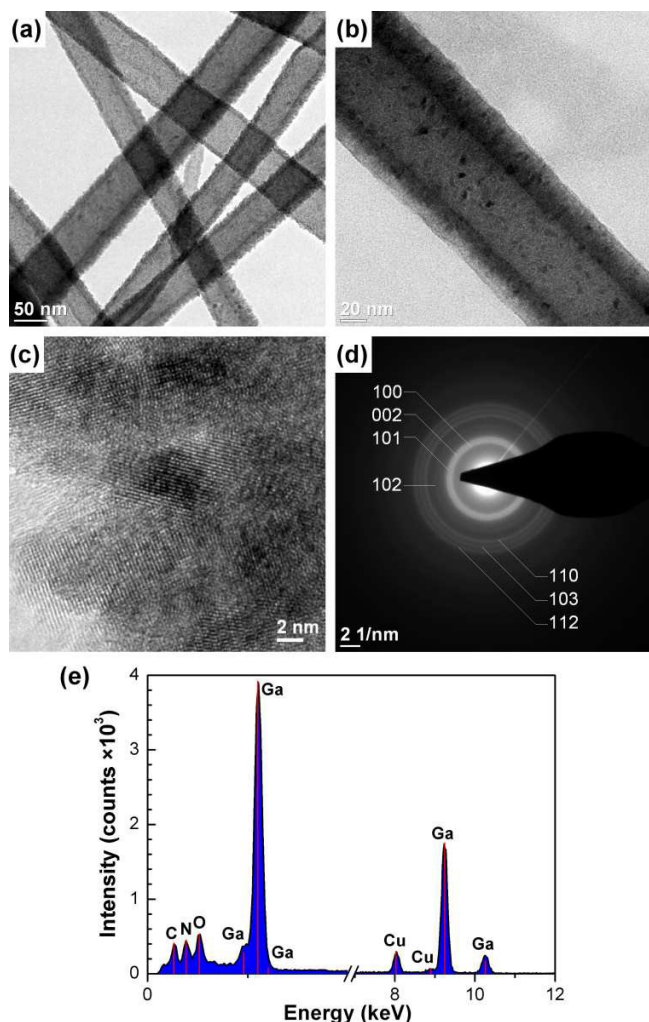


Figure 2. Representative (a, b) TEM, (c) high-resolution TEM images, (d) SAED pattern, and (e) EDX spectrum of nylon-GaN core-shell nanofiber(s).

impractical. The ideal purging time, which is closely related to precursor dose, exposure time and temperature, should be long enough to avoid the overlap of different precursor molecules. On the other hand, it should be short enough to avoid desorption of precursor molecules from the substrate surface. Both of the above extreme conditions would impair the uniformity and conformality, and make accurate sub-Å thickness control impossible. Above all, the precursor molecules should be able to reach every single point on the substrate to be coated. For 3D substrates with high aspect ratios, this means that enough time should be allowed for precursor molecules to reach the deepest corners of the substrate.⁵⁸ This is usually done by exposing the substrate to precursor molecules for a certain period of time under the static vacuum condition; i.e., the so called “*exposure mode*” (a trademark of Ultratech/Cambridge Nanotech Inc.).⁴⁵ In the exposure mode, dynamic vacuum is switched to static vacuum just before each precursor pulse by closing the valve between the reaction chamber and the pump, allowing the substrate to be exposed to precursor molecules for a certain

period of time (i.e., exposure time). This is followed by a purging period, where the chamber is switched back to dynamic vacuum for efficient evacuation/purging of excess precursor molecules and gaseous byproducts. At this point, it should also be noted that the plasma-assisted ALD is known to be inferior to thermal ALD in terms of conformality due to radical recombination; therefore it does not benefit from the exposure mode as much as the thermal ALD does.⁵⁹ Since the GaN HCPA-ALD process has not yet been optimized for the high surface area 3D nanofiber mats, TEM investigation indicated thickness variation and/or less than expected deposition for this process. Nevertheless, the highly uniform and conformal deposition of thin GaN layers on every single electrospun nanofiber in a mat with a certain surface area and thickness can easily be envisioned by simply using the correct process parameters in the light of the information given above.

Structural characterization of the deposited GaN layer was also conducted during the TEM study. Figure 2c is a high-resolution TEM image of the GaN shell of a nylon-GaN core-shell nanofiber. The image shows a polycrystalline structure with ≤ 15 nm-sized crystals. The polycrystalline structure was also evidenced in the SAED measurements. The pattern obtained (Figure 2d) consists of polycrystalline diffraction rings, corresponding to the wurtzite (hexagonal) GaN (*h*-GaN) crystal structure. Measured ring diameters, theoretical values for *h*-GaN and the corresponding crystallographic planes are summarized in Table 1. The first ring from the center was quite thick; therefore, the inner and outer diameters of this ring were measured and found to be 6.948 nm^{-1} and 8.553 nm^{-1} , corresponding to (100) and (101) planes with calculated interplanar spacing (d_{hkl}) values of 2.879 \AA and 2.338 \AA , respectively. The diffraction ring corresponding to (002) plane of *h*-GaN ($d_{hkl} = 2.593 \text{ \AA}$) was also apparent in this relatively thick diffraction ring, however it is not distinguishable due to the merging of three individual diffraction rings. It should also be noted that when the same HCPA-ALD recipe was deposited on planar Si substrates, six of these seven reflections of the *h*-GaN phase appeared in the grazing-incidence XRD pattern.⁵⁴ The presence of GaN was further confirmed by an EDX analysis performed on the TEM

Table 1. SAED results, theoretical values and corresponding crystallographic planes.

Diameter (nm^{-1})	Interplanar spacing, d_{hkl} (\AA)		Corresponding plane, hkl
	calculated	theoretical ^a	
6.948	2.879	2.7620	100
8.553	2.338	2.4370	101
10.483	1.9079	1.8910	102
12.494	1.6008	1.5945	110
13.591	1.4716	1.4649	103
14.749	1.3560	1.3582	112

^aHexagonal GaN, ICDD reference code: 00-025-1133.

sample (see Figure 2e), which indicated the presence of Ga due to the GaN shell, N due to the GaN shell and/or nylon core, and C and O due to the nylon core. We note that a fraction of contribution to C and O might be originated from atmospheric contamination. On the other hand oxidation of the GaN surface might also contribute to the intensity of O signal. The Cu signal in the EDX spectrum is due to the Cu TEM grid.

XRD patterns of the pristine nylon 6,6 and nylon-GaN core-shell nanofibers are given in Figure 3. For these measurements, both nanofiber mats were peeled off from their supports (i.e., Al foil) and placed on a zero-background XRD sample holder. Nylon 6,6 may exist in various crystalline forms; i.e., α , β , or γ -phase.⁶⁰ The XRD pattern of the pristine nylon 6,6 nanofibers exhibited two distinct diffraction peaks at $\sim 20.2^\circ$ (100) and $\sim 22.6^\circ$ (010, 110) and thereby confirmed the presence of α phase.^{60,61} The $\alpha 1$ peak is related with the distance between the hydrogen-bonded chains, whereas the $\alpha 2$ peak corresponds to the separation of hydrogen-bonded sheets.⁶⁰ The absence of the reflections of β phase at 2θ values of $\sim 12^\circ$ and $\sim 19^\circ$ or $\gamma 1$ peak ($2\theta = \sim 13^\circ$) and $\gamma 2$ peak ($2\theta = \sim 22^\circ$)⁶⁰ indicates that the nylon 6,6 nanofibers in the electrospun mat have a pure triclinic α phase comprising hydrogen-bonded sheets.⁶² The peaks corresponding to the α phase of nylon 6,6 were also apparent in the XRD pattern of nylon-GaN core-shell nanofiber mat. However, in addition, we also observed peaks corresponding to the *h*-GaN phase. The reflections (100), (002), (101), and (110) of the *h*-GaN phase appeared at $\sim 2\theta$ values of 32.2° , 34.1° , 36.6° , and 57.5° , respectively. These results are in very good agreement with the SAED results given in Figure 2d and Table 1.

Chemical compositions and bonding states of the pristine nylon 6,6 and nylon-GaN core-shell nanofibers were studied using XPS. XPS survey scans of pristine nylon 6,6 and nylon-GaN core-shell nanofibers are given in Figure 4a. Survey spectrum of the pristine nylon 6,6 nanofibers indicated the presence of N, C and O elements as anticipated. Elemental composition of the sample was determined by the

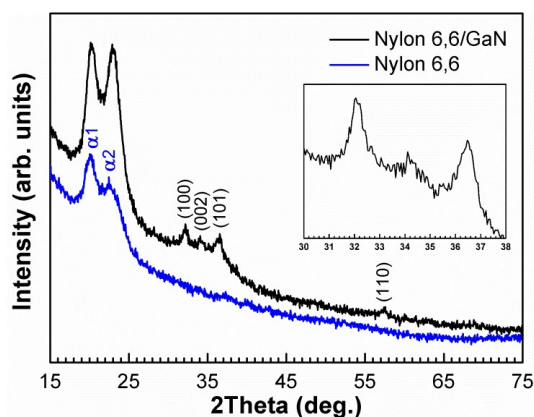


Figure 3. XRD patterns of freestanding pristine nylon 6,6 and nylon-GaN core-shell nanofibers. The inset shows the XRD pattern of freestanding nylon-GaN core-shell nanofiber mat recorded with an exaggerated counting time (i.e., 2000 s) within the 2θ range of 30 – 38° .

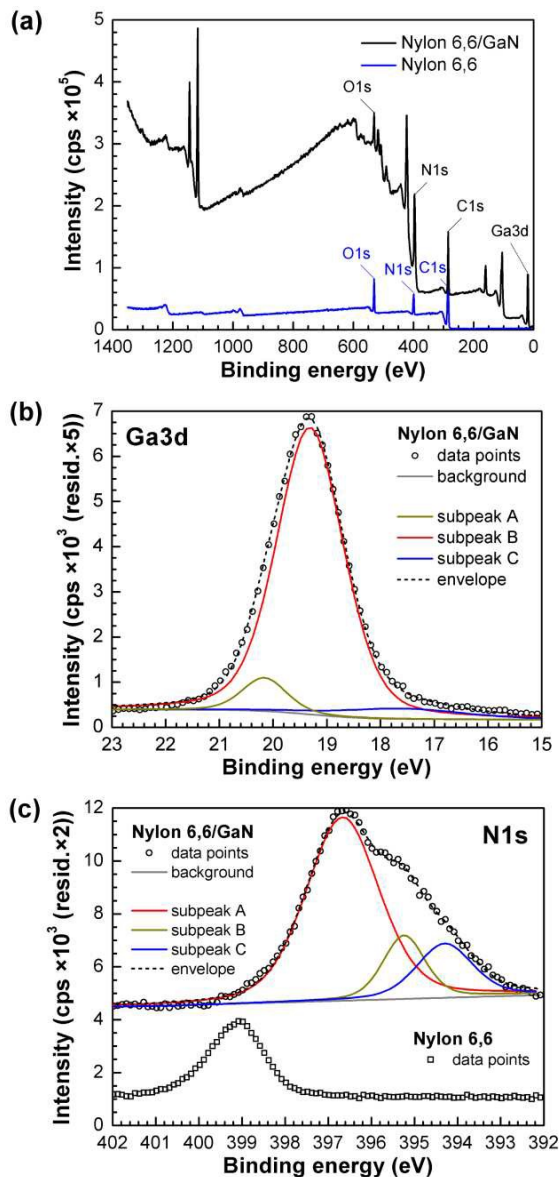


Figure 4. (a) XPS wide energy survey scans of pristine nylon 6,6 and nylon-GaN core-shell nanofibers. (b) Ga3d high-resolution XPS scan of nylon-GaN core-shell nanofibers, and (c) N1s high-resolution XPS scans of pristine nylon 6,6 and nylon-GaN core-shell nanofibers.

quantification of this spectrum as 11.52 at.% N, 76.92 at.% C and 11.56 at.% O, which is quite close to the theoretical values of 12.5 at.% N, 75 at.% C and 12.5 at.% O.⁶³ For the nylon-GaN core-shell nanofibers, on the other hand, 20.95 at.% Ga, 28.20 at.% N, 38.22 at.% C, and 12.64 at.% O were detected. It should be noted that for the GaN thin film deposited on a Si substrate at the same temperature using identical HCPA-ALD parameters, XPS survey scan detected 7.92 at.% C on the film surface. As have already been discussed in a previous study,²³ a relatively large X-ray beam interacts ($\sim 400 \mu\text{m}$ spot size) with a large number of core-shell nanofibers during the analysis, which might have discontinuities or cracks on the shell layer due to the method of sample preparation. Therefore, although XPS is a surface

analysis technique that collects data from the top ~5-10 nm depending on the material, it should not be surprising in an XPS analysis to observe signal(s) from the underlying core. Therefore, the C, N and O amounts reported here should be considered as a collective of the nylon core and GaN shell, with a smaller contribution from the former. Figure 4b is the Ga3d high-resolution XPS scan of nylon-GaN core-shell nanofibers, which was fitted similar to its thin film counterpart⁵⁴ using three subpeaks located at 20.16 eV (subpeak A), 19.31 eV (subpeak B) and 17.63 eV (subpeak C). Subpeaks A and B were assigned to the Ga-O^{64,65} and Ga-N^{64,65,66} bonds, respectively, whereas subpeak C was found to be related to the contribution from the N2s core level.^{65,67} N1s high-resolution XPS scans of pristine nylon 6,6 and nylon-GaN core-shell nanofibers are shown in Figure 4c. High-resolution XPS spectrum of pristine nylon 6,6 nanofibers exhibited a peak at ~399 eV, which is assigned as the NCO, amide bond.⁶³ This peak is absent in the high-resolution XPS spectrum of nylon-GaN core-shell nanofibers, which was fitted by three subpeaks located at 396.67 eV (subpeak A), 395.24 eV (subpeak B) and 394.30 eV (subpeak C). Subpeak A corresponds to the N-Ga bond,⁶⁸ whereas subpeaks B and C were identified as the Auger Ga peaks.⁶⁹ Note that the high-resolution N1s scan of the GaN film deposited on a Si substrate via HCPA-ALD at the same temperature was also fitted using three subpeaks having locations similar to those reported here for nylon-GaN core-shell nanofibers.⁵⁴

Characteristics PL emission spectra of ~20 nm-thick GaN thin film deposited on Si, pristine nylon 6,6 nanofibers and nylon-GaN core-shell nanofibers are given in Figure 5. The GaN spectrum (Figure 5a) exhibited a broad spectral feature centered at 368 nm, which results from the main band gap emission in GaN thin film. The less steeper slope in the 400-450 nm spectral region, on the other hand, might be designated to bulk and surface related impurities and/or defect structures. As seen in Figure 5b, two emission peaks were observed at 336 nm and between 418 and 440 nm for pristine nylon 6,6 nanofibers. Relative PL intensity of the pristine nylon 6,6 nanofibers was significantly higher than that detected for the GaN thin film sample. Although the observed emission at low wavelengths was not strong for the nylon-GaN core-shell nanofibers (Figure 5c), PL intensity detected at 450 nm was significantly higher than those recorded from pristine nylon 6,6 nanofibers and GaN thin film.

The representative photograph of the fabricated nylon-GaN core-shell nanofiber mat is given in Figure 6. The fabricated mat was easily peeled off from its support (i.e., Al foil); moreover, it was easily handled and folded due to its flexible profile in the freestanding state. Mechanical properties of pristine nylon 6,6 and nylon-GaN core-shell nanofiber mats were investigated by dynamic mechanical analysis (DMA). Tensile test results are summarized in Table S1. The nylon-GaN core-shell nanofiber mat exhibited significantly poor tensile properties as compared to those of

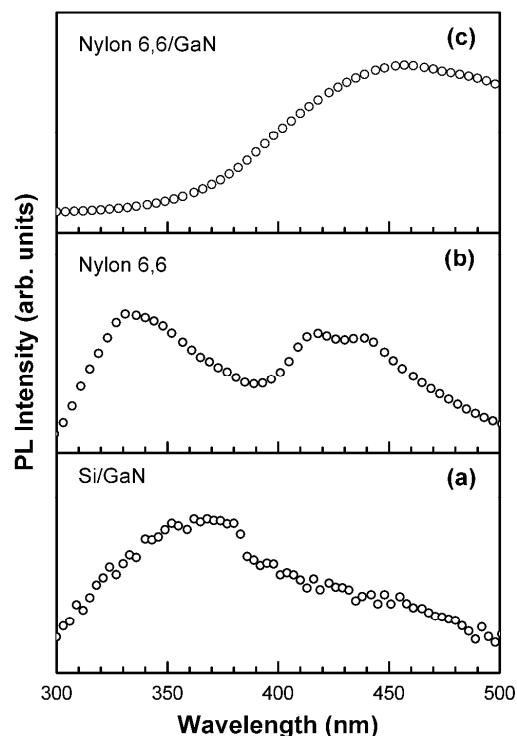


Figure 5. PL emission spectra of (a) ~20 nm-thick GaN thin film deposited on Si, (b) pristine nylon 6,6 nanofibers, and (c) nylon-GaN core-shell nanofibers.

pristine nylon 6,6 nanofiber mat. However, the hybrid nanofibrous structure responded to applied stress with proportional strain (see Figure S1(a)), indicating an elastic behavior. The storage moduli of nanofiber mats are given in Figure S1(b) as a function of temperature. The storage modulus values of both samples decreased within the temperature range of 75-200 °C due to the segmental motion of polymer chains. The storage modulus of pristine nylon 6,6 nanofiber mat was observed to be higher than that of the hybrid nanofiber mat, indicating deteriorated mechanical properties for nylon-GaN core-shell nanofibers. The difference between the mechanical behaviors of two samples is possibly because of inorganic nature of GaN shell part, which lead to reduction at the elastic feature of pristine nylon

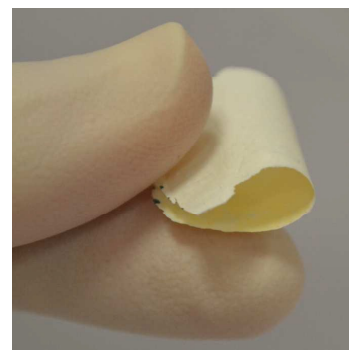


Figure 6. The representative photograph of the freestanding nylon-GaN core-shell nanofiber mat. The fabricated mat can easily be handled and folded owing to the flexible organic cores.

nanofibers; in addition, slight degradation of polymeric core is also quite possible since nylon 6,6 core exposed to 200 °C for an extended period of time (~17 h) in ALD chamber. Nevertheless, DMA results show that these polymer-GaN hybrid nanofibers fabricated by the combination of electrospinning and HCPA-ALD processes exhibit decent mechanical integrity for practical applications. In addition, the inherent mechanical properties of pristine nylon 6,6 nanofiber mat could be maintained for the fabricated hybrid nanostructures by simply lowering the HCPA-ALD temperature of the GaN shell layer.

Conclusions

Polymer (nylon 6,6)-GaN core-shell nanofibers were fabricated by the combination of electrospinning and HCPA-ALD processes. Morphological investigation carried out using SEM revealed bead-free nylon 6,6 nanofibers with an average fiber diameter of ~70 nm. Subsequently deposited GaN layer perfectly replicated the fiber morphology of polymeric 3D substrate, forming nylon-GaN core-shell nanofibers with an average fiber diameter of ~123 nm. TEM studies showed slightly non-uniform or less than expected thicknesses for the GaN layers on nylon 6,6 nanofibers, indicating the need for the optimization of HCPA-ALD process parameters such as precursor doses, exposure time and purging time for these high specific surface area 3D substrates with a very high aspect ratio. The presence of GaN on nylon 6,6 nanofibers was evidenced by elemental analyses carried out using EDX and XPS. High-resolution Ga3d and N1s XPS spectra revealed Ga-N and N-Ga bonding states with peaks located at 19.31 eV and 396.67 eV, respectively. The structure of the GaN shell layer was examined using high-resolution TEM, SAED and XRD, all of which indicated a polycrystalline layer with wurtzite crystal structure. Nylon-GaN core-shell nanofiber mats were easily handled in their freestanding state owing to their flexible cores and showed satisfying mechanical integrity as determined DMA. Moreover, the flexible core-shell GaN nanostructures were fabricated at a processing temperature (i.e., 200 °C) much lower than those needed for the preparation of GaN nanofibers using conventional techniques. These organic-inorganic semiconducting nanofibers, therefore, have potential to substitute brittle ceramic GaN nanofibers in various electronic and optoelectronic devices such as gas sensors and UV photodetectors.

Acknowledgements

S. Vempati thanks The Scientific and Technological Research Council of Turkey (TUBITAK) (TUBITAK-BIDEB 2221, Fellowships for Visiting Scientists and Scientists on Sabbatical) for fellowship. E. Goldenberg gratefully acknowledges the financial support from TUBITAK (TUBITAK-BIDEB 2232, Project # 113C020). N. Biyikli thanks EU FP7-Marie Curie-IRG for funding NEMSmart (PIRG05-GA-2009-249196). T. Uyar thanks EU

FP7-Marie Curie-IRG (NANOWEB, PIRG06-GA-2009-256428) and The Turkish Academy of Sciences-Outstanding Young Scientists Award Program (TUBA-GEBIP) for partial funding. M. Guler from UNAM is acknowledged for TEM imaging.

Notes and references

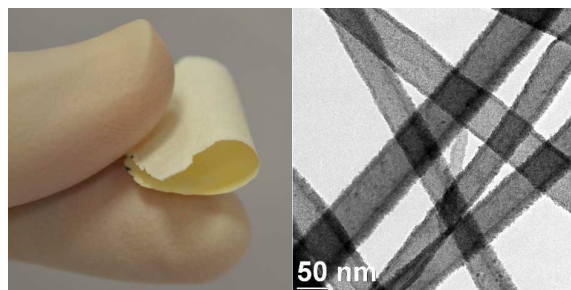
^aUNAM-National Nanotechnology Research Center, Bilkent University, Ankara, 06800, Turkey.

^bInstitute of Materials Science and Nanotechnology, Bilkent University, Ankara, 06800, Turkey.

E-mail: ozgit@bilkent.edu.tr, biyikli@unam.bilkent.edu.tr

1. S. C. Jain, M. Willander, J. Narayan and R. Van Overstraeten, *J. Appl. Phys.*, 2000, **87**, 965–1006.
2. S. Barth, F. Hernandez-Ramirez, J. D. Holmes and A. Romano-Rodriguez, *Prog. Mater. Sci.*, 2010, **55**, 563–627.
3. C.-C. Chen, C.-C. Yeh, C.-H. Chen, M.-Y. Yu, H.-L. Liu, J.-J. Wu, K.-H. Chen, L.-C. Chen, J.-Y. Peng and Y.-F. Chen, *J. Am. Chem. Soc.*, 2001, **123**, 2791–2798.
4. Z. Zhong, F. Qian, D. Wang and C. M. Lieber, *Nano Lett.*, 2003, **3**, 343–346.
5. T. Kuykendall, P. J. Pauzauskie, Y. Zhang, J. Goldberger, D. Sirbully, J. Denlinger and P. Yang, *Nat. Mater.*, 2004, **3**, 524–528.
6. C.-C. Chen and C.-C. Yeh, *Adv. Mater.*, 2000, **12**, 738–741.
7. F. Qian, Y. Li, S. Gradečak, D. Wang, C. J. Barrelet and C. M. Lieber, *Nano Lett.*, 2004, **4**, 1975–1979.
8. B. Xu, D. Yang, F. Wang, J. Liang, S. Ma and X. Liu, *Appl. Phys. Lett.*, 2006, **89**, 074106.
9. X. Duan and C. M. Lieber, *J. Am. Chem. Soc.*, 2000, **122**, 188–189.
10. Y. Huang, X. Duan, Y. Cui and C. M. Lieber, *Nano Lett.*, 2002, **2**, 101–104.
11. G. S. Cheng, L. D. Zhang, Y. Zhu, G. T. Fei, L. Li, C. M. Mo and Y. Q. Mao, *Appl. Phys. Lett.*, 1999, **75**, 2455–2457.
12. J. Goldberger, R. He, Y. Zhang, S. Lee, H. Yan, H.-J. Choi and P. Yang, *Nature*, 2003, **422**, 599–602.
13. C. Youtsey, L. T. Romano and I. Adesida, *Appl. Phys. Lett.*, 1998, **73**, 797–799.
14. K. J. Lee, J. Lee, H. Hwang, Z. J. Reitmeier, R. F. Davis, J. A. Rogers and R. G. Nuzzo, *Small*, 2005, **1**, 1164–1168.
15. A. Meléndez, K. Morales, I. Ramos, E. Campo and J. J. Santiago-Avilés, *9th IEEE Conf. Nanotechnol.*, 2009, **5394610**, 269–272.
16. A. Meléndez, K. Morales, I. Ramos, E. Campo and J. J. Santiago-Avilés, *Proc. SPIE - Int. Soc. Opt. Eng.*, 2009, **7402**, 740210.
17. J. L. Robles-García, A. Meléndez, D. Yates, J. J. Santiago-Avilés, I. Ramos and E. M. Campo, *Proc. SPIE - Int. Soc. Opt. Eng.*, 2011, **8036**, 80360F.
18. E. M. Campo, J. Poplawsky, A. Meléndez, J. L. Robles-García, I. Ramos, D. Yates, J. E. Fischer and J. J. Santiago-Avilés, *RSC Adv.*, 2014, **4**, 2634–2639.
19. E. M. Campo, A. Meléndez, K. Morales, J. Poplawsky, J. J. Santiago-Avilés and I. Ramos, *Proc. SPIE - Int. Soc. Opt. Eng.*, 2010, **7729**, 77290T.
20. H. Wu, Y. Sun, D. Lin, R. Zhang, C. Zhang and W. Pan, *Adv. Mater.*, 2009, **21**, 227–231.
21. X. Luo, X. Zheng, D. Wang, Y. Zhang, H. Cheng, X. Wang, H. Zhuang and Y. Lou, *Sensors Actuators B Chem.*, 2014, **202**, 1010–1018.
22. Q. Peng, X.-Y. Sun, J. C. Spagnola, G. K. Hyde, R. J. Spontak and G. N. Parsons, *Nano Lett.*, 2007, **7**, 719–722.

23. C. Ozgit-Akgun, F. Kayaci, I. Donmez, T. Uyar and N. Biyikli, *J. Am. Ceram. Soc.*, 2013, **96**, 916–922.
24. A. Haider, C. Ozgit-Akgun, F. Kayaci, A. K. Okyay, T. Uyar and N. Biyikli, *APL Mater.*, 2014, **2**, 096109.
25. I. Donmez, F. Kayaci, C. Ozgit-Akgun, T. Uyar and N. Biyikli, *J. Alloys Compd.*, 2013, **559**, 146–151.
26. B.-S. Lee, W.-S. Kim, D.-H. Kim, H.-C. Kim, S.-H. Hong and W.-R. Yu, *Smart Mater. Struct.*, 2011, **20**, 105019.
27. W.-S. Kim, B.-S. Lee, D.-H. Kim, H.-C. Kim, W.-R. Yu and S.-H. Hong, *Nanotechnology*, 2010, **21**, 245605.
28. G. M. Kim, S.-M. Lee, G. H. Michler, H. Roggendorf, U. Gösele and M. Knez, *Chem. Mater.*, 2008, **20**, 3085–3091.
29. S.-W. Choi, J. Y. Park, C. Lee, J. G. Lee and S. S. Kim, *J. Am. Ceram. Soc.*, 2011, **94**, 1974–1977.
30. A. Katoch, J.-H. Kim and S. S. Kim, *ACS Appl. Mater. Interfaces*, 2014, **6**, 21494–21499.
31. J. Y. Park, S.-W. Choi and S. S. Kim, *Nanotechnology*, 2010, **21**, 475601.
32. S. Cho, D.-H. Kim, B.-S. Lee, J. Jung, W.-R. Yu, S.-H. Hong and S. Lee, *Sensors Actuators B Chem.*, 2012, **162**, 300–306.
33. A. Katoch, S.-W. Choi and S. S. Kim, *Nanotechnology*, 2014, **25**, 455504.
34. G.-M. Kim, S.-M. Lee, M. Knez and P. Simon, *Thin Solid Films*, 2014, **562**, 291–298.
35. A. Katoch, S.-W. Choi, G.-J. Sun, H. W. Kim and S. S. Kim, *Nanotechnology*, 2014, **25**, 175501.
36. E. Santala, M. Kemell, M. Leskelä and M. Ritala, *Nanotechnology*, 2009, **20**, 035602.
37. A. A. Chaaya, M. Bechelany, S. Balme and P. Miele, *J. Mater. Chem. A Mater. Energy Sustain.*, 2014, **2**, 20650–20658.
38. S.-W. Choi, J. Y. Park and S. S. Kim, *Nanotechnology*, 2009, **20**, 465603.
39. J. Y. Park, S.-W. Choi, J.-W. Lee, C. Lee and S. S. Kim, *J. Am. Ceram. Soc.*, 2009, **92**, 2551–2554.
40. F. Kayaci, S. Vempati, C. Ozgit-Akgun, I. Donmez, N. Biyikli and T. Uyar, *Nanoscale*, 2014, **6**, 5735–5745.
41. I. M. Szilágyi, E. Santala, M. Heikkilä, V. Pore, M. Kemell, T. Nikitin, G. Teucher, T. Firkala, L. Khriachtchev, M. Räsänen, M. Ritala and M. Leskelä, *Chem. Vap. Depos.*, 2013, **19**, 149–155.
42. Q. Du, J. Wu and H. Yang, *ACS Catal.*, 2014, **4**, 144–151.
43. Q. Peng, X.-Y. Sun, J. C. Spagnola, C. Saquing, S. A. Khan, R. J. Spontak and G. N. Parsons, *ACS Nano*, 2009, **3**, 546–554.
44. F. Kayaci, C. Ozgit-Akgun, I. Donmez, N. Biyikli and T. Uyar, *ACS Appl. Mater. Interfaces*, 2012, **4**, 6185–6194.
45. F. Kayaci, C. Ozgit-Akgun, N. Biyikli and T. Uyar, *RSC Adv.*, 2013, **3**, 6817–6820.
46. F. Kayaci, S. Vempati, C. Ozgit-Akgun, N. Biyikli and T. Uyar, *Appl. Catal. B Environ.*, 2014, **156–157**, 173–183.
47. F. Kayaci, S. Vempati, I. Donmez, N. Biyikli and T. Uyar, *Nanoscale*, 2014, **6**, 10224–10234.
48. M. Asif Khan, R. A. Skogman, J. M. Van Hove, D. T. Olson and J. N. Kuznia, *Appl. Phys. Lett.*, 1992, **60**, 1366–1368.
49. N. H. Karam, T. Parodos, P. Colter, D. McNulty, W. Rowland, J. Schetzina, N. El-Masry and S. M. Bedair, *Appl. Phys. Lett.*, 1995, **67**, 94–96.
50. Y. Kumagai, M. Mayumi, A. Koukitsu and H. Seki, *Appl. Surf. Sci.*, 2000, **159–160**, 427–431.
51. O. H. Kim, D. Kim and T. Anderson, *J. Vac. Sci. Technol. A*, 2009, **27**, 923–928.
52. C. Ozgit, I. Donmez, M. Alevli and N. Biyikli, *J. Vac. Sci. Technol. A*, 2012, **30**, 01A124.
53. C. Ozgit-Akgun, I. Donmez and N. Biyikli, *ECS Trans.*, 2013, **58**, 289–297.
54. C. Ozgit-Akgun, E. Goldenberg, A. K. Okyay and N. Biyikli, *J. Mater. Chem. C*, 2014, **2**, 2123–2136.
55. S. Bolat, C. Ozgit-Akgun, B. Tekcan, N. Biyikli and A. K. Okyay, *Appl. Phys. Lett.*, 2014, **104**, 243505.
56. B. Tekcan, C. Ozgit-Akgun, S. Bolat, N. Biyikli and A. K. Okyay, *Opt. Eng.*, 2014, **53**, 107106.
57. A. Baji, Y.-W. Mai, S.-C. Wong, M. Abtahi and X. Du, *Compos. Sci. Technol.*, 2010, **70**, 1401–1409.
58. R. G. Gordon, D. Hausmann, E. Kim and J. Shepard, *Chem. Vap. Depos.*, 2003, **9**, 73–78.
59. J. Musschoot, J. Dendooven, D. Deduytsche, J. Haemers, G. Buyle and C. Detavernier, *Surf. Coatings Technol.*, 2012, **206**, 4511–4517.
60. J. Li, Y. Zuo, X. Cheng, W. Yang, H. Wang and Y. Li, *J. Mater. Sci. Mater. Med.*, 2009, **20**, 1031–1038.
61. C. P. Leo, A. Linggawati, A. W. Mohammad and Z. Ghazali, *J. Appl. Polym. Sci.*, 2011, **122**, 3339–3350.
62. Q. Zhang, Z.-Z. Yu, M. Yang, J. Ma and Y.-W. Mai, *J. Polym. Sci. Part B Polym. Phys.*, 2003, **41**, 2861–2869.
63. M. C. Burrell and J. J. Chera, *Surf. Sci. Spectra*, 1999, **6**, 13–17.
64. S. D. Wolter, B. P. Luther, D. L. Waltemyer, C. Önnby, S. E. Mohny and R. J. Molnar, *Appl. Phys. Lett.*, 1997, **70**, 2156–2158.
65. V. Matolin, S. Fabik, J. Glosik, L. Bideux, Y. Ould-Metidji and B. Gruzza, *Vacuum*, 2004, **76**, 471–476.
66. P. Kumar, M. Kumar, Govind, B. R. Mehta and S. M. Shivaprasad, *Appl. Surf. Sci.*, 2009, **256**, 517–520.
67. W. R. L. Lambrecht, B. Segall, S. Strite, G. Martin, A. Agarwal, H. Morkoç and A. Rockett, *Phys. Rev. B*, 1994, **50**, 14155–14160.
68. Z. Majlinger, a. Bozanic, M. Petravica, K.-J. Kim, B. Kim and Y.-W. Yang, *Vacuum*, 2009, **84**, 41–44.
69. G. Moldovan, I. Harrison, M. Roe and P. D. Brown, *Inst. Phys. Conf. Ser.*, 2004, **179**, 115–118.



Flexible polymer-GaN nanofibers were fabricated at a temperature much lower than those needed for the preparation of GaN ceramic nanofibers.